Electronic Supplementary Information (ESI) for:

Enhancement of Static Incubation Time in Microfluidic Cell Culture Platforms Exploiting Extended Air-Liquid Interface

Nilanjana Bose[1], Tamal Das[1], Debapriya Chakraborty[2], Tapas K. Maiti[1], Suman Chakraborty[2,*]

[1]Department of Biotechnology, Indian Institute of Technology, Kharagpur, India – 721302

[2]Department of Mechanical Engineering, Indian Institute of Technology, Kharagpur, India – 721302

1. Development of the Microfluidic Platform

In this section, we have introduced the basic protocol for fabrication of an extended air-liquid two-phase patterned surface in PDMS based microdevice with the aid of laminar flow. We have characterized the formation of "virtual wall" (air-liquid interface) by optimizing the parameters related to the patterning of the inner surfaces of the microdevice.

1.1 Preparation of Microdevice

1.1.1 Microdevice Geometry Design and Fabrication

A mask for the Y-shaped microchannel is drawn using AutoCAD software (AutoCAD, Autodesk) and printed with high resolution on a transparency sheet. The transparency is used as a mask in photolithography to create a master mold. A negative photoresist SU-8-2075 (MicroChem Corp, Newton, MA, USA) is spin-coated on standard glass slide (cleaned by piranha solution, H_2SO_4: H_2O_2 = 1:1 by volume) at 4000 rpm for 20s. The coated photoresist is exposed to ultra-violet (UV) light through the photomask for 30s. Subsequently, it is developed using SU8 developer (MicroChem Corp, Newton, MA, USA), followed by rinsing in isopropyl alcohol and drying with nitrogen flow to obtain a mold of Y-shaped channel. A mixture of PDMS base to cross-linker (Sylgard 184, Dow Corning) in a ratio of 10:1 w/w is poured onto the

---

[*] Corresponding Author, email: suman@mech.iitkgp.ernet.in

mold, degassed, heated at 70 °C for 30 min and subsequently peeled off the mold to make the PDMS stamp containing negative replica of Y-shaped channel.

1.1.2 Chemical Treatment (Solvent Extraction) of PDMS Stamps

PDMS has an inherent hydrophobic nature with aqueous solvents and make the surface prone to non-specific adsorption to proteins and other biomolecules (such as hormones). The solution to this problem is encountered by oxidizing the PDMS surface in oxygen plasma for a min or less, rendering the surface hydrophilic. However, rearrangements of the uncured bulk of PDMS oligomers to the surface of PDMS reverts back the hydrophobicity within 30 min. This recovery of PDMS may be postponed to one week through serial solvent extraction method, in which the uncured oligomers within the PDMS were removed [1]. The PDMS stamps were treated and extracted in a series of solvents designed to remove unreacted oligomers from the bulk phase followed by oxygen plasma treatment. For extraction, molded PDMS stamps were immersed in 200 ml of triethylamine solution at 25°C and allowed to stir for 2 hr. Subsequently, the same stamps were placed in 200ml of ethyl acetate at 25°C for 2 hr with stirring, replacing with fresh solvent after 1 hr. Finally, the PDMS stamps were placed in 200 ml of acetone again for 2 hr. The stamps were allowed to dry completely in at 70 °C for 6 hr.

1.1.3 Total Assembled Microdevice

After the surface modification of the PDMS stamps, inlet and outlet ports were punched by a blunt end 20-gauge needle. The PDMS stamps were then plasma-oxidized and bonded irreversibly to piranha-cleaned glass slides. After bonding the stamps to the glass slides, the needles were placed in the holes. A small amount of PDMS mixture was applied to the cylindrical surface of the needles. The PDMS mixture slowly settled down near the junction. The whole setup was then immediately heated for 10-15 mins at 70°C. A piece of micropipette tip was cut with at least one planar surface and bonded to the PDMS stamp with a small amount of uncured PDMS mixture. It was then placed centering the needles and heated for 20 mins at 70°C. This makes the reservoirs at the inlet and outlet. PDMS mixture was poured into the reservoirs around the syringe needle tips and was heated at 70°C for 25-30 mins until the supports became rigid for inlet A and B in Fig. 1. The silicone tubings were connected to the open end of needles, and the other ends were connected to a syringe pump.

1.1.4 Patterning inside Microdevice

Each of the inlets of the PDMS microdevice was connected to the syringe pump (Harvard Apparatus PHD 2000 Programmable,USA) via silicon tubing filled with the desired solution and the flow was achieved by pressure-driven flow mechanism. Pure stream of hexadecane and octadecyltrichlorosilane (OTS) [2] solution ($C\%$ v/v in hexadecane) was passed through each inlets of the microdevice with the aid of syringe pump. The flow was laminar and was maintained at a flow rate Q_H ml/min for time t mins. The flow of the solvents were followed by sequential flushing with hexane and isopropanol and then dried with flow of nitrogen gas. The top and bottom surfaces of the microdevice exposed to OTS solution became hydrophobic with the formation of self-assembled monolayers (SAM) of OTS on the surface. The other region through which only hexadecane flowed remained hydrophilic. Liquid was passed and confined at the hydrophilic region. The liquid subsequently passed at the hydrophilic side was sustained strongly by the "virtual wall" i.e. air-liquid interface which was formed at the midway of the microdevice.

2. Mathematical Modeling

2.1 Strength of the Virtual Wall

For shallow microchannels (H<<w), the flow field may be modelled using standard Hele-Shaw approximations, implying that the spatial variations along the depth (z-direction) are much faster than along the width (y-direction) and length of the microchannel (x-direction). The average velocity may be obtained by depth averaging as: $\vec{v}(x,y,z) = -\left(1 - \frac{z^2}{H^2}\right)\frac{H^2}{3\eta}\vec{\nabla}p$ in the limit of the low Reynolds number and under steady state. The velocity may be integrated over the cross-section to obtain the average flow rate (Q) along the hydrophilic region. The gradient of pressure is estimated using $\Delta P_h \big/ L$ where ΔP_h is the hydrostatic pressure head (difference in the inlet and outlet pressures) and L is the axial length of the microchannel. Hence, we obtain the axial pressure difference as: $\Delta p_h = \frac{72QL\mu}{AH^2}$ where A is the cross sectional area of the hydrophilic region. This pressure of the fluid tries to spread the fluid throughout the channel, while the

3

pressure due to surface tension opposes at the air-liquid interface. The pressure difference across the interface may be obtained from the Laplace equation as: $\Delta p_l = \sigma \left(\dfrac{1}{R_1} + \dfrac{1}{R_2} \right)$, where σ is the liquid-vapor surface tension coefficient, R_1 and R_2 are the radii of curvature in two perpendicular planes (x-y plane and y-z plane) of the interface. The radius of curvature on x-y plane is very large and may be ignored while the radius of curvature on y-z plane may be obtained as R. From Fig.S1, it may be easily deduced that the radius of curvature of the virtual wall is related to the height of the microchannel as [2]: $R = \dfrac{H}{2\sin\left(\theta - \pi/2\right)}$ where θ is static contact angle. Finally, the Laplace pressure may be obtained as $\Delta p_l = \dfrac{2\sigma \sin\left(\theta - \pi/2\right)}{H}$. Hence, the critical parameter β may be expressed as the ratio of the hydrostatic pressure: $\Delta p_h = \dfrac{72QL\mu}{AH^2}$ to the Laplace pressure:

$\Delta p_l = \dfrac{2\sigma \sin\left(\theta - \pi/2\right)}{H}$. When the flow rate of fluid is increased so that the parameter $\beta > O(1)$ (where $O(1)$ refers to order 1), the hydrostatic pressure (acting due to axial flow) increases over the Laplace pressure and the virtual wall gets damaged. If the flow rate is decreased below the threshold limit $\beta < O(1)$, the Laplace pressure supports the fluidic head and the interface remains sustained. Hence, the parameter β is an indicator of the strength of the virtual wall. It is important to note that the interface remains stationary when the flow rate is maintained below the critical limit and hence the contact angle θ is taken as the static contact angle. If $\beta > O(1)$, the interface gets disturbed and displaced from the equilibrium. However, as the liquid pressure head is withdrawn, the hydrophobic region pushes back the interface to the equilibrium, and the contact angle with the substrate is no longer static. We characterize both static and dynamic contact angles in the subsequent section using goniometer (See Section 3).
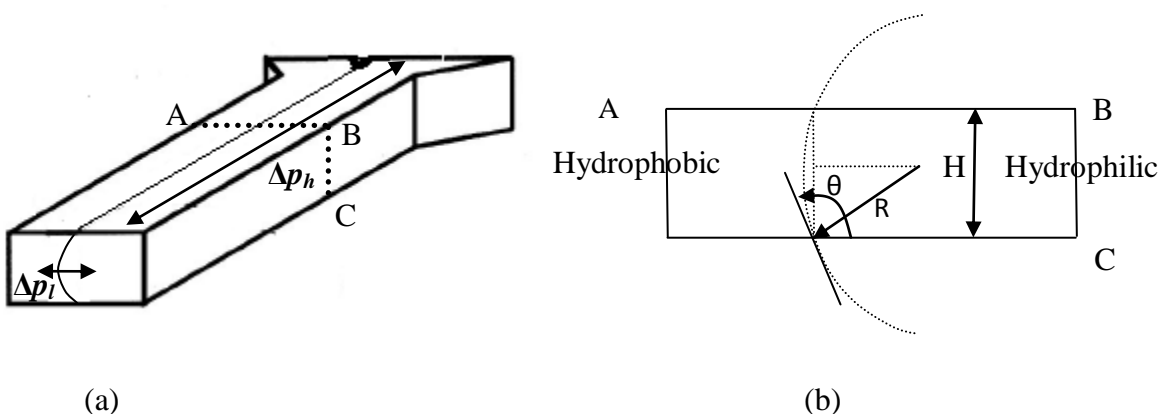
(a)   (b)

Fig. S1 (a) The schematic of the microchannel showing the axial pressure Δp_h and the transverse pressure Δp_l, (b) Side view of the microdevice showing the interface in dotted lines, separating hydrophobic and hydrophilic regions. R is the radius of the curvature of the meniscus, H is the height of the microdevice and θ is the contact angle.

2.2 Oxygen Concentration

The motivation behind the creation of the virtual wall in the present study was to provide a continuous supply of gaseous oxygen (O_2) which could replenish the limited oxygen concentration by lateral diffusion in the aqueous media during prolonged culture of cells. The diffusion of oxygen across the virtual wall into the media confined at the hydrophilic region has been studied using nondimensionalised species conservation equation: $\frac{\partial C}{\partial t} = \left(\frac{\partial^2 C}{\partial y^2} + \frac{\partial^2 C}{\partial z^2} \right)$ where

C is the concentration of oxygen as nondimensionalised by C_0 (the concentration of oxygen in air) , y and z are the spatial coordinates along the transverse direction and depth of the microchannel respectively (considering the cross- section of the channel) nondimensionalised by the length scale L (=width 2 mm), and t is the time nondimensionalised by reference diffusion time scale $\frac{L^2}{D}$ where D (=10^{-10}m²/s) is the diffusion coefficient of the oxygen in the media. Typically, the diffusion time scale turns out to be approximately 11 hrs. As the cell culture period is of the order of days, the distribution of the oxygen across the width of the channel

remains uniform in most of the experiments. The consumption of O_2 at one of the surfaces containing cells is modeled using Michaelis-Menten kinetics and is represented as:

$$\frac{\partial C}{\partial z} = Da \frac{C}{k_m + C}$$ at $z=0$ (glass surface containing cells) where Da is the Damkohler number representing the ratio of the oxygen uptake rate to the diffusion rate, k_m is the Michaelis-Menten constant nondimensionalised by C_0. At $y=0$ we consider $C = 1$ (concentration of oxygen in the gas side) for the case of virtual wall and no flux condition for the case of actual wall, to compare the diffusion of oxygen through the virtual wall. At the physical walls, $y=1$ and $z = 1$ we implement no species flux boundary condition. For the purpose of simulation, we have taken the initial concentration in the media to be 0.6, the value Da to be of the order of 10^{-3} and k_m to be 0.05 [3]. We have represented the average concentration of the oxygen for the presence of actual wall in Fig. S2 (a) and with virtual wall in Fig. S2 (b). In Fig. S2 (a), we observe the decrease of concentration of oxygen for different aspect ratios of the channels ($\varepsilon=$ height/width of the microchannel), because of the consumption by cells adhered to the surface for actual wall. It was observed that for low aspect ratio channels, the depletion of the oxygen in the media is very fast which is detrimental for the cells and hampers cell growth. In contrast, we can see from Fig. S2(b) that the replenishment of oxygen in the media with the presence of virtual wall is very fast and maintains a constant value equal to that of the concentration of oxygen on other side of the virtual wall irrespective of the aspect ratio of the microchannel. Hence, the present approach provides an efficient way of controlling the concentration of gases (not limited to oxygen only) in media dynamically.
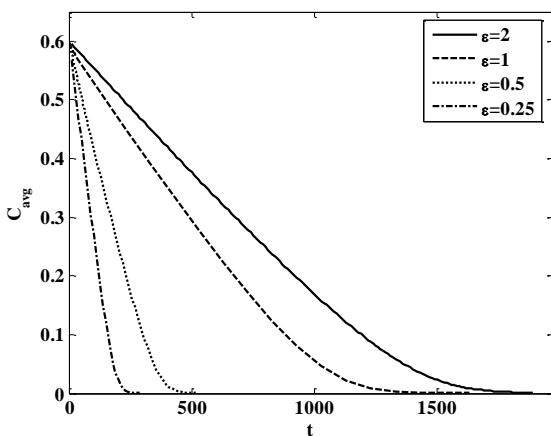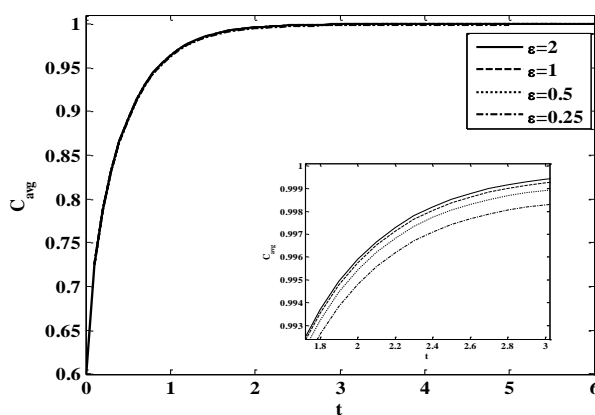
(a)   (b)

Fig. S2 Variations of average concentration in the domain as a function of time (t) - (a) Actual wall (b) Virtual wall, where C_{avg} is the area weighted average of the domain in consideration

3. Interface Characterization

3.1 Contact Angle Measurement

Self-Assembled Monolayer (SAM) of OTS has been deposited onto the inner surfaces of the microdevice to render it hydrophobic by laminar flow of OTS solution unlike the traditional means of dipping the substrate into silane solutions. The deposition of monolayers onto the inner surfaces was measured by indirect ways with the critical flow rate of liquid, expressed as β. However, we have employed a direct approach to characterize the modified patterned surface by measuring the contact angles (static and dynamic) and related hysteresis of the substrate. Both static and dynamic contact angles of water on patterned PDMS microdevice were measured using goniometer. Measurements were carried out at room temperature and the distilled water was used as a probing liquid.

3.1.1 Static Contact Angle Measurement

The static contact angle was measured at the cross-section of the device where the interface is located at the centre of the device. A series of ten measurements were attained to calculate an average static contact angle. The static contact angle at the interface was observed 106.6˚ as shown in the inset of fig S3.

3.1.2 Dynamic Contact Angle Measurement

In dynamic contact angle measurements, two different types of contact angles are measured. The angle measured during the advancement of a contact line or wetting of the surface is referred as the advancing contact angle, whereas, the angle measured during the receding of the contact line is referred as the receding contact angle. In order to measure the dynamic contact angle of the PDMS surface, we have used a micro-dispenser which was programmed to dispense fluid and retract the fluid volume of the probing fluid to measure advancing and receding contact angles at a rate of 12 μL/min. A typical dynamic contact angle measurement on the patterned

PDMS is shown in Fig. S3. The difference between advancing and receding contact angles is termed as a contact angle hysteresis which is typically in the range of 5°-20° [4]. Here, the advancing contact angle on patterned surface dropped from approximately 110° to 105°, whereas the receding contact angle decreased from 105° back to 98°. The change in contact angle near the interface is less than 12° after repeated experiments with moving contact lines as shown in the figure (Fig. S3). Small change in contact angle near the interface reflects less hysteresis of the substrate and the stability of the interface. Perturbations in pressure during the flow of aqueous solvents in confined situation near the virtual wall (interface) could damage the virtual wall. The inherent nature of the hydrophobic surface forces the solvent to retract back to the hydrophilic region, thereby leading to a decay of these perturbations at the interface. However if the contact angle hysteresis is large, the above effect is going to reduce after repeated use. In our present situation, because of less hysteresis, this device could sustain the virtual wall for prolonged period of time, most suitable for long term cell culture.
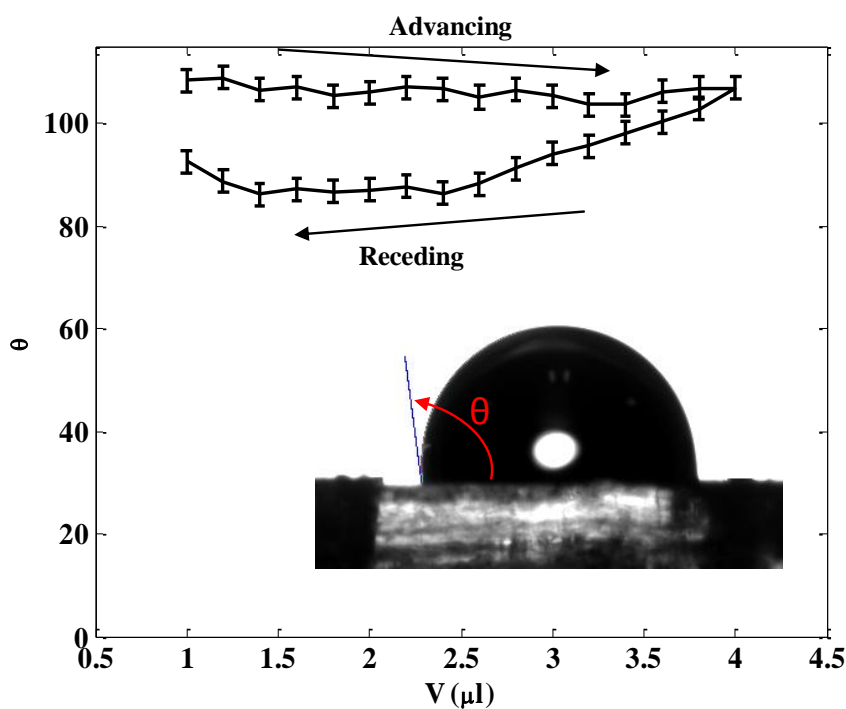

Fig. S3 Advancing and receding water contact angle (θ) as a function of droplet volume (V μl) on the patterned surface. The inset shows the static contact angle of a drop over the patterned surface.

4. Cell Related Studies

4.1 Materials and Methods

Mouse fibroblast cell line L929 and embryonic fibroblast NIH3T3 (obtained from the National Centre for Cell Sciences, Pune, India) were maintained in Dulbecco's Modified Essential Medium (DMEM, GIBCO, Gaithersburg, MD) and RPMI-1640 (GIBCO, Gaithersburg, MD) respectively, supplemented with 2 mM glutamine, 100 U ml^{-1} penicillin, 0.1 mg ml^{-1} streptomycin (GIBCO, Gaithersburg, MD), and 10% heat-inactivated fetal bovine serum. Human osteosarcoma cell line MG63 was maintained as a monolayer culture in Minimum Essential Medium (MEM, HyClone, India) and supplemented with 2 mM L-glutamine, 1.0 mM sodium pyruvate, and 10% heat-inactivated fetal bovine serum. These cells were cultured with regular passages in a CO_2 incubator (Heraeus, Germany) at 37ºC and 5% CO_2. L929 and NIH3T3 cells are fibroblast in origin whereas MG63 cells are human osteosarcoma cells. All these cell lines are adherent in nature and are cultured on 25cm^2 area cell culture flask. Cells were trypsinized followed by centrifugation at 1000rpm for 10mins and resuspending in fresh medium. Cell concentration was determined using Haemocytometer.

Before cell seeding inside the patterned microdevice, 10μg/ml of fibronectin solution was prepared by dissolving 1mg of fibronectin in 1ml phosphate saline buffer (PBS, pH= 7.4). The hydrophilic pathway of the patterned microdevice was treated with the fibronectin solution and incubated at 37°C for 2 hr. Treatment with the fibronectin solution was followed by washing the surface with PBS for 2 to 3 times. The time required by cells to adhere onto surface of the microchannels was found to be more than 8 hrs without surface activation [5]. However, surface activation promotes cellular attachment to the extracellular matrix (ECM). Next, different representative cells at a concentration of 10^{5}cells/ml were injected inside the microdevice by a syringe pump. Each cell type has been cultured in separate microdevice. Same number of cells was seeded in control sets. The control microchannels were non-patterned PDMS microchannels and with dimensions of 25 mm length, 1 mm width (same as the width of hydrophilic region of patterned microchannel) and 40 μm height.

Cells of the microdevice and control microchannels have been incubated and maintained at all times in incubator with controlled environment. Cells have been incubated inside an

incubator (Heraeus, Germany) at 37 °C in a humidified atmosphere containing 5% CO_2, to maintain the physiological temperature and pH of the cell culture. After overnight incubation of the cells of the microdevice and control microchannels inside the humidified CO_2 incubator, cells are taken outside the incubator only for time-lapse imaging in phase-contrast inverted microscope (IX-71, Olympus, Germany). All the imaging studies (cell proliferation study, cell culture and cell viability) have been performed in a CO_2 microscope stage incubator (Olympus, MIU-IBC-IF, Germany) with appropriate conditions (37°C and 5% CO_2) for cell cultures right on the microscope stage, thus allowing prolonged observations of cell events in a controlled environment. This eliminates the influences of the external or ambient atmosphere (non-physiological environmental conditions) on the performance of the cell culture in the microdevice as well as in control microchannels. The imaging of the cells in both the microdevice and control microchannels was performed intermittently at regular intervals for growth kinetics study. After the images of the cells were taken in phase-contrast microscope, the microdevice and the control microchannels were again kept inside the CO_2 incubator for long-term cell culture. Images were further analyzed by the combination of an image processing software (Image-Pro Plus, Media Cybernetics) and Matlab (MathWorks) image processing features. For study of cell adhesion, cell proliferation and growth kinetics of cells in the microdevice, phase-contrast images were taken and each image has been divided into several sub frames of 300μm x 300μm area. The cells were counted in each sub-frame and were averaged to get the total number of cells at a given location of the microdevice. The growth kinetics of the cells in control microchannels were compared to that of the microdevice cell culture.

4.2 Investigation of the Cytocompatibility of the Microdevice

Cytocompatibility of two-phase patterned microdevice was investigated by monitoring the cell adhesion and cell proliferation study of 3T3 cells. 3T3 fibroblast cells (10^5cells/ml) were seeded into the microdevice and incubated in an incubator. The volume of the hydrophilic region was 6μl and contained about 600 cells during seeding. Both the cell adhesion and cell proliferation were observed under phase contrast inverted microscope.

4.2.1 Axial distribution of cells

We have observed that the distribution of cells after adhesion is not uniform across the microchannel although distribution of cells during the seeding was uniform. In order to investigate the reason behind this, we have varied different pertinent parameters – Reynolds number (Re) during the seeding, height of the microchannel (H) and the volume of the media in the outlet reservoir. The adhesion distribution of the cells was calculated along the axial distance of the microdevice (x) normalized by the total length of the microdevice (l) by obtaining phase-contrast images of the same. Subsequently, each frame of the images was analyzed by dividing into several bins (or sub-frames). The number of the cells (N) per unit area attached in each bin was counted and averaged to yield the number of cells attached per unit area of the microdevice at a given axial location. All the cell numbers are normalized by the maximum number of cells (N_{max}). The first two parameters – Re and H have no influence on the distribution of the cells as may be observed in Fig. S4 (a, b). However, the effect of media volume at the outlet reservoir may be attributable to the non-uniform axial distribution of the cells as shown in the Fig. S4 (c). The outlet media reservoir is important for long-term cell culture to supplement the consumed nutrient. The presence of outlet reservoir results in initial axial non-uniform distribution of the cells. Cells adhere more near the reservoir than that of the other locations of the microchannel as shown in Fig. S4 (c), where the outlet reservoir is located at $x/l=1$. During initial adhering period, cells have a preference towards the outlet because the reservoir facilitates more supplements than that of the locations near the inlet. The blue circled region show nearly uniform number of cells and has been considered for the cell proliferation study in order to observe more precisely the direct effects of the air-liquid interface on the survival of the cells as shown in Fig. S5.
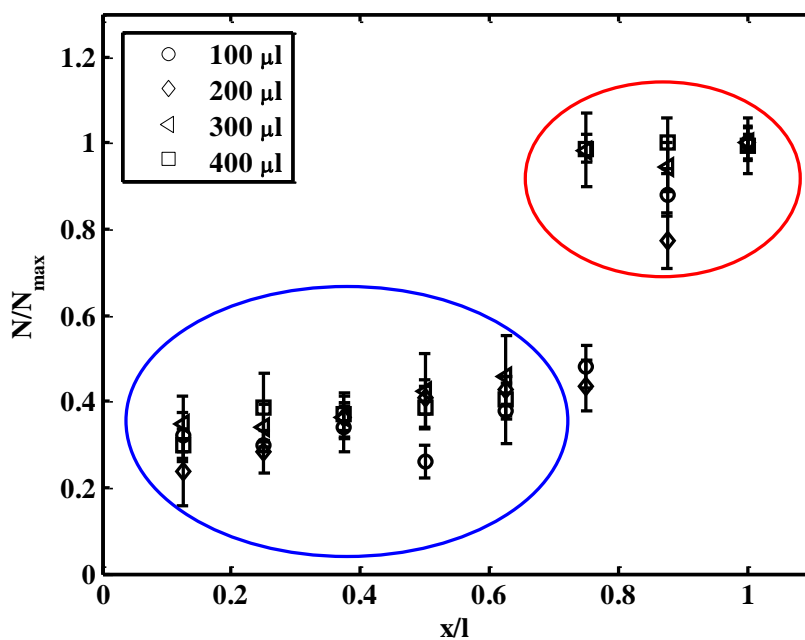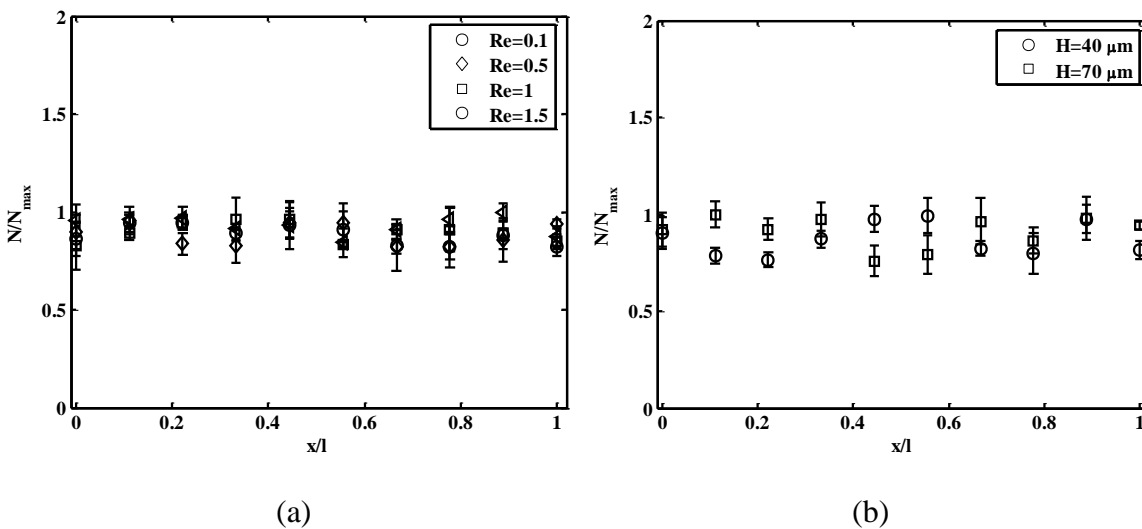
11

Fig. S4 Axial distribution of cells in the microfluidic device for- (a) different Reynolds numbers (*Re*) and (b) different heights of the microchannel (*H*). Number of cells (*N*) has been counted at each bin located at different axial locations and non-dimensionalised by the maximum number of cells (N_{max}). (c) Effect of the volume of the media in the reservoir (located at the outlet) on the axial distribution of the cell in the microchannel. Cell encircled in red is near the outlet reservoir, where the outlet reservoir is located at x/l=1. Cells encircled in blue are considered to evaluate the proliferation study.

4.2.2. Proliferation Study

The cells were monitored at regular intervals and their growth kinetics was studied for about 96 hrs in a static condition (without external media replenishment). Here, all cell proliferation data have been normalized with respect to the initial adhered cell number present after 12 hours of seeding (N_0), i.e., allowing sufficient time for cell adhesion yet not long enough for cells to undergo cell division cycle. We have varied the concentration of the OTS for patterning to observe the effect on cell proliferation. The cells that have been cultured in the microchannel, modified with 2% OTS concentration, have shown statistically significant growth in comparison to all the remaining patterned and control microchannels as shown as shown in Fig. S5. The maximum growth ratio obtained from this data (Fig. S5) is used to represent Fig. 3 in the main text. At lower concentration of OTS (<2%), the interface is not stable and growth resembles to that of the control (non-patterned microchannel). At higher concentrations of OTS (>2%), the toxic effects are manifested after prolonged incubation resulting in decreased growth rate. In order to confirm this effect, we have obtained the distribution of live and dead cells for 20% OTS concentration as shown in Fig. S6. Although there is cell proliferation, the toxic effects of the hydrophobic side with prolonged incubation results in the dead cells to be more concentrated near the interface ($y=0$).
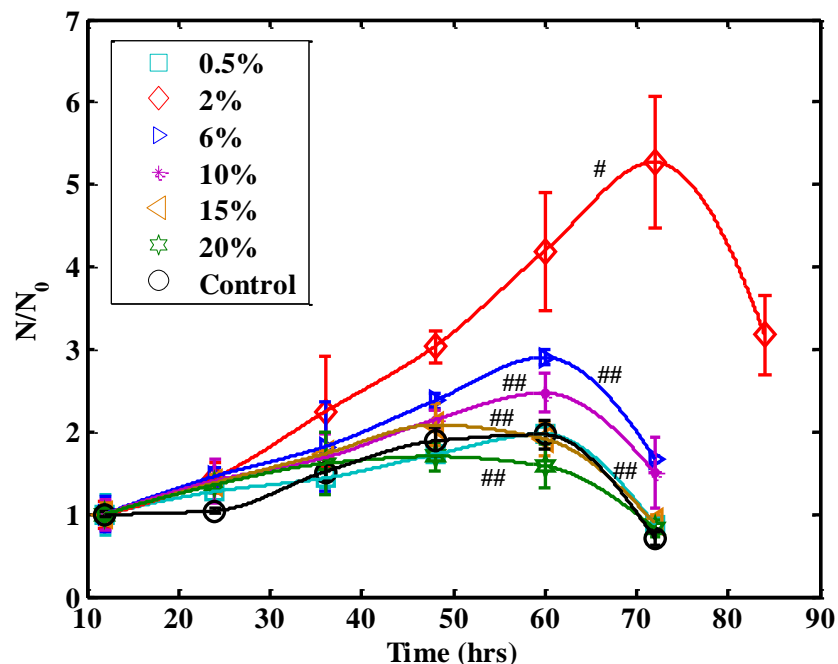
Fig. S5 Proliferation Study of 3T3 fibroblast cells in the microdevice with two-phase interface as a function of time of incubation for different concentrations of OTS (*C%*) used for patterning the inner surfaces of the microdevice. A non-patterned microchannel of identical dimensions of the hydrophilic region served as a control. The errorbars show the standard deviation corresponding to each dataset for n=5 (number of experiments). # refers to $p<0.05$ while ## refers to $p>0.05$ significance with respect to control.
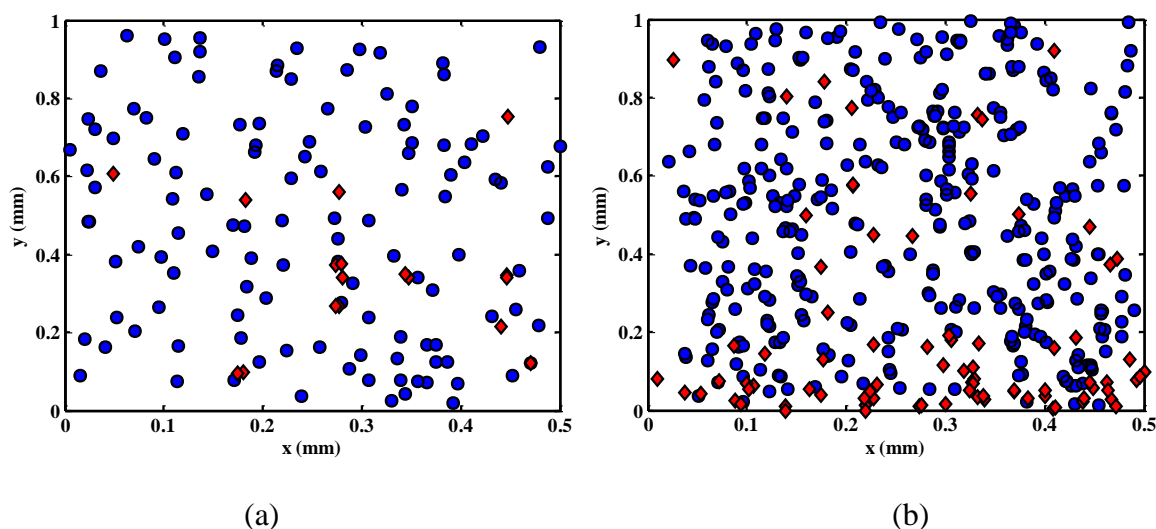

(a)   (b)

Fig. S6 Distribution of live and dead cells for 20% OTS patterned microchannel, where *y=0* and *y=1mm* represent the position of the air-liquid interface and channel wall respectively at (a) 12 hrs (b) 48 hrs after cell seeding. ● represents the location of the live cell and ◆ represents the location of dead cell.

14

4.2.3 Comparative Study with different cell lines

Three different types of biological cell lines- L929 (murine fibroblast cells), 3T3 (murine embryonic fibroblast) and MG63 (human osteosarcoma) were taken as representative cell lines for cell culture in our microdevice in static condition and without media perfusion (see Fig. 4 in main text). During seeding, the flow rate has been maintained at <1μl/min for 15 mins until the cells were evenly distributed along the length of the microdevice. A comparative study among L929, 3T3 and MG63 cells in the microdevice has been shown in Fig. 4 in the main text.

References

1. J. A. Vickers, M. M. Caulum, and C. S. Henry, Anal. Chem. 2006, 78, 7446-7452
2. B. Zhao, J. S. Moore, and D. J. Beebe, Science, 2001, 291, 1023-1026; Anal. Chem., 2002, 74, 4259-4268
3. N. Korin, A. Bransky, U. Dinnar and S. Levenberg, Lab Chip, 2007, 7, 611-617
4. P. R. Waghmare, and S. K. Mitra, Langmuir, 2010, 26, 17082–17089
5. T. Das, T. K. Maiti, and S. Chakraborty, Lab Chip, 2008, 8, 1308–1318